Nonlocal-thermal-equilibrium model of a pulsed capillary discharge waveguide

B. H. P. Broks, K. Garloff, and J. J. A. M. van der Mullen*
Department of Applied Physics, Eindhoven University of Technology, P.O. Box 513, 5600 MD Eindhoven, The Netherlands
(Received 16 July 2004; revised manuscript received 24 September 2004; published 3 January 2005)

Slow pulsed capillary discharges are under investigation for use as plasma channel waveguides in laser-wakefield acceleration. In this study, we present a non-local thermal equilibrium (non-LTE) plasma model with a model for the wall temperature coupled to it. This model is used to describe an example of a slow pulsed capillary discharge, and the results are compared with experimental results. The agreement is satisfactory, indicating suitability of our model. Significant deviations from LTE are found during the formation of the plasma channel. The model is also used to study the influence of the discharge current on the guiding properties. It was found that this influence is small over most of the current range that was investigated.

DOI: 10.1103/PhysRevE.71.016401 PACS number(s): 52.65.Kj, 52.80.Tn, 52.38.Hb, 52.30.Ex

I. INTRODUCTION

Laser-wakefield acceleration is an acceleration technique that makes it possible to build relatively compact particle accelerators by the virtue of the large acceleration gradients that are created [1]. For this application, it is critical that the laser is focused to a small spot size and kept as a narrow bundle over a length of several cm. This requirement means that the laser must not diffract over many Raleigh diffraction lengths [2]. This can be achieved by channeling the laser beam through a suitably formed plasma. For a Gaussian beam, the channeling is optimal when the electron density of the plasma has a hollow parabolic shape, with the lowest density in the center. In this arrangement, the refractive index of the plasma provides a guiding that is similar to that in gradient index fiberoptics [3].

It is also important that the plasma is fully ionized, meaning that every atom is stripped of all its electrons, in the parts where it will interact with the laser. Not fully ionized particles will be further ionized by the laser, consuming laser power and disturbing the electron density profile.

One of the methods used for creating a suitable plasma is the capillary discharge. There are several types of these discharges in use.

Discharge-ablated capillaries operate by ablating and subsequently ionizing wall material [4]. This obviously limits the lifetime of the capillary. Furthermore, the relatively low temperature causes less than full ionization.

An alternative is the fast gas-filled capillary discharge. The gas used should be easy to fully ionize, such as hydrogen. A current pulse, typically several tens of kA during tens of nanoseconds, creates a pinch plasma. This current produces a plasma that is suitable as a waveguide [5–7]. However, the azimuthal magnetic field not only produces the pinch, but also makes the channel susceptible to MHD instabilities [3].

Using a lower current for a longer time reduces the MHD instabilities significantly. A working waveguide based on this principle, called a slow capillary discharge, has been demonstrated [8]. These discharges have a diameter of a few hundred microns, are filled with several kPa of hydrogen, and are ionized by a current pulse of a few hundred A lasting a few hundred ns. They are wall-stabilized. The typical current densities of 10^9 A m^{-2} are much more than conventional steady-state arcs, which operate at about 10^6 A m^{-2}, but much less than pinch plasmas, where the current density can reach values of 10^{11} A m^{-2}.

In this study, a model will be presented that is valid for these slow capillary discharges. This model will be used to simulate an actual waveguide, and the simulated results will be compared with experimental results. The physics behind the formation of the channel and the suitability for guiding of the found electron density profile will be discussed. Our model will be compared with an earlier model given in Bobrova *et al.* [9] where the same device is modeled. Our model differs on three key points, namely in the treatment of the wall, the treatment of the nonequilibrium aspects and the composition calculation. It will be shown that nonequilibrium aspects have an important impact on the formation of the hollow electrondensity profile. The model is then used to investigate the influence of the discharge current on the plasma guiding properties.

II. THE PHYSICAL MODEL

Based on the type of discharge, which is basically a pulsed wall-stabilized high-current hydrogen arc discharge, we will create a physical model to describe the system, and justify the assumptions used to arrive at this model.

The system consists of two regions, the discharge plasma and the wall. They are described by different models, coupled by the boundary conditions.

A. The model of the plasma

The basis of the plasma model is formed by a two-temperature non-LTE quasineutral fluid model, which is used extensively in the description of low-temperature plasmas and has a wide range of validity. This model is described by the following equations:

(i) The bulk continuity equation,

*Electronic address: j.j.a.m.v.d.mullen@tue.nl

$$\frac{\partial \rho}{\partial t} + \vec{\nabla} \cdot (\rho \vec{v}) = 0. \quad (1)$$

Here, ρ is the bulk density, t is the time and $\vec{v}$ is the bulk velocity.

(ii) The bulk momentum conservation equation,

$$\frac{\partial \rho \vec{v}}{\partial t} + \vec{\nabla} \cdot (\rho \vec{v} \vec{v}) = -\vec{\nabla} p + \vec{F}_{\mathrm{Lor}} - \vec{\nabla} \cdot (\mu \vec{\nabla} \vec{v}). \quad (2)$$

Here, p is the bulk pressure, $\vec{F}_{\mathrm{Lor}}$ is the Lorentz force, and μ is the viscosity.

(iii) The species conservation equation,

$$\frac{\partial n_i}{\partial t} + \vec{\nabla} \cdot (n_i \vec{v}) = \sum_j S_j R_{ji}. \quad (3)$$

Here, n_i is the density of species i, S_j is the reaction rate for reaction j and R_{ji} is the stoichiometric constant of the production of particle i by reaction j.

(iv) The electron energy equation,

$$\frac{\partial C_e T_e}{\partial t} + \vec{\nabla} \cdot [(C_e T_e + p_e)\vec{v}] - \vec{v} \cdot \vec{\nabla} p_e - \vec{\nabla} \cdot (\lambda_e \vec{\nabla} Te) = -k_{\mathrm{heat}}(T_e - T_h) + \frac{J^2}{\sigma} - \sum_j \Delta E_j S_j. \quad (4)$$

Here, C_e is the electron heat capacity, T_e is the electron temperature, p_e is the electron pressure, λ_e is the electron heat conductivity, k_{heat} is elastic electron-heavy particle heat transfer rate, T_h is the heavy particle temperature, J is the current density, σ is the conductivity, and ΔE_j is the reaction energy for reaction j.

(v) The heavy particle energy equation,

$$\frac{\partial C_h T_h}{\partial t} + \vec{\nabla} \cdot ((C_h T_h + p_h)\vec{v}) - \vec{v} \cdot \vec{\nabla} p_h - \vec{\nabla} \cdot (\lambda_h \vec{\nabla} Th) + \bar{\bar{\tau}} : \vec{\nabla} \vec{v} = k_{\mathrm{heat}}(T_e - T_h). \quad (5)$$

Here, C_h is the heavy particle heat capacity, p_h is the heavy particle pressure, λ_h is the heavy particle heat conductivity, and $\bar{\bar{\tau}}$ is the viscosity tensor.

Equations (1) and (2) describe the bulk behavior of the system. From these equations, the velocity field and pressure are computed. The non-LTE chemistry, which can contain as many chemical species and reactions between these species as necessary, is solved with a set of equations (3). In this non-LTE approach, it is assumed that all the heavy particles share a common temperature T_h and the electrons have a possibly different temperature T_e. We use Eq. (5) to compute the former and Eq. (4) to compute the latter. Because we assume that all the Ohmic heating is done by the electrons and that all the reactions are due to electron kinetics, these source terms are solely in the electron energy balance and not in the heavy particle balance.

In principle, the capillary discharge is two-dimensional, having a radial symmetry. However, since the length of the capillary is typically two orders of magnitude larger than its radius, we expect that the discharge can be described well by assuming it only depends on the radial coordinate r and the time t.

B. Source terms and transport coefficients

We will now discuss the meaning and validity of these equations, and present the formulas for the transport coefficients and source terms.

Equation (1) is the continuity equation, which does not contain source terms or transport coefficients.

Equation (2) is a special case of the Navier–Stokes equation with only one bulk force, $\vec{F}_{\mathrm{Lor}}$. This force is caused by the current in the axial z direction generating a magnetic field B in the ϕ direction. This results in $\vec{F}_{\mathrm{Lor}}$ (in the negative r-direction) of which the magnitude F_{Lor} is given by

$$F_{\mathrm{Lor}} = JB. \quad (6)$$

The magnetic field is obtained by using Ampère's law,

$$B = \frac{\mu J r}{2}. \quad (7)$$

The magnetic permeability μ is assumed to be equal to the magnetic permeability of vacuum $\mu_0 = 4\pi \times 10^7$ F m^{-1}. The viscosity in the last term of Eq. (2) is computed based on the description in Ref. [10]. However, we correct the Coulomb logarithm λ for the effects of plasma nonideality as outlined in Ref. [11]:

$$\lambda = \ln(0.6\Lambda) \quad (8)$$

with Λ the ratio of the Debye length and the impact parameter [10]. We use this corrected Coulomb logarithm throughout this work. The difference between the corrected and uncorrected Coulomb logarithm is at most 30%. In this plasma, the ion Hall parameter is always much smaller than 1, so the magnetization of the ions has a negligible influence on the transport parameters.

In our model, the following four species are used: the heavy particles H_2, H, H^+ and the electrons e. We note that the actual number of species in the plasma is much larger than the four species we take into account: the plasma also contains among others excited hydrogen molecules and atoms, and hydrogen molecular ions. The small energy distance between these excited states and the ion state, combined with the relatively high electron temperature, causes the destruction of these species to be rapid. The formationon the other hand is slower due to the larger energy gap between the ground state and the excited states. Therefore, their density is low and we do not take them into account explicitly. For hydrogen molecular ions, fast dissociative recombination reactions cause a similar depletion.

To obtain the non-LTE chemical composition, the species conservation equation (3) is solved for two species, the electron density is obtained from quasineutrality, and the last species follows from the bulk pressure obtained from Eq. (1) and Eq. (2) [12]. The right-hand side of Eq. (3) represents the sources from the reactions. We take into account three reactions and their inverse reactions.

(i) Electron impact dissociation,

$$H_2 + e \rightarrow 2H + e. \tag{9}$$

The rate coefficient k_{ediss} for this reaction is determined using the cross sections in Ref. [13], noting that the high electron temperature causes the direct process to be faster than the stepwise process. We found that the rate coefficient between an electron temperature of 1.5 eV and 3.5 eV can be approximated satisfactorily by a modified Arrhenius rate k,

$$k = c\left(\frac{T_e}{\text{eV}}\right)^q \exp\left(\frac{-E}{k_B T_e}\right) \tag{10}$$

with $q=2$, $c=1.41\times10^{-15}$ m^3 s^{-1} and E the reaction energy of 4.5 eV. While the temperature in the plasma will rise beyond this range, the dissociation of H_3 is complete at that time, so the poor description of this reaction for these high temperatures is not important. We neglect dissociation by heavy particles, as the heavy particle temperature does not rise high enough to significantly dissociate hydrogen before virtually all hydrogen is dissociated by electron impact dissociation.

(ii) Direct electron impact ionization

$$H + e \rightarrow H^+ + 2e. \tag{11}$$

The rate coefficient for this reaction is obtained from [14], and fitted with an Arrhenius rate Eq. (10) with $c=7.1\times10^{-15}$ m^3 s^{-1}, $q=0.4$ and $E=13.6$ eV.

(iii) Stepwise electron impact ionization. Ionization can also take place from an excited state to the ion state. This reaction is generally a lot faster than ionization from the ground state. In this case the rate-determining step becomes excitation fromthe ground state to the first excited state [15] (this process is of lesser importance in lower-density plasmas, as the radiative decay of the excited state may prevent ionization). Using the cross sections from Ref. [14], the excitation rate from the ground state to the first excited state, and thus the rate of stepwise ionization, can be approximated by Eq. (10) with $c=1.24\times10^{-14}$ m^3 s^{-1}, $q=0.3$, and $E=10.6$ eV. A similar process may occur for excitation to and subsequent ionization from the second or even higher excited state However, as the cross sections are smaller and the energy gaps are bigger for excitation to higher excited states, these processes are slower (typically by orders of magnitude) than stepwise ionization via the first excited state. Stepwise processes to higher excited states are therefore not taken into account.

For all processes, the reverse process rates are computed using detailed balancing.

Note that in Eq. (3) diffusion losses are not taken into account. In order to verify the assumption that diffusion is negligible, we will estimate the diffusion frequency with

$$\nu_{\text{diff}} = \frac{D}{L^2}, \tag{12}$$

where D is the diffusion coefficient and L a typical length scale. The typical diffusion coefficients are in the order of 0.1 m^2 s^{-1}, while the typical diffusion length can be approximated by the radius of the channel. Thus, we obtain a typical loss frequency in the order of 10^7 Hz. This is small compared to the typical frequencies at which species are formed and destroyed, which are in the order of 10^5–10^9 Hz. Hence, we can ignore diffusion and still expect reasonable results.

Equation (4) is used to compute the electron temperature field. The first term of this equation describes the temporal behavior of the heat content of the electron gas, in which we used

$$C_e = \tfrac{3}{2}k_B n_e \tag{13}$$

with k_B Boltzmann's constant. This assumes that the electons behave as a perfect gas. The electron heat conductivity λ_e is obtained from the Frost mixture rules [16]. These are valid-provided the electron Hall parameter is much smaller than unity. This condition is satisfied during most of the discharge, albeit only marginally during the first 10 ns. The heat transfer rate k_{heat} is determined using Ref. [10], ignoring the effect of the inelastic collisions of electrons with molecular hydrogen. The conductivity σ is computed using the Frost mixture rules.

The last term in Eq. (4) is the contribution to the electron heat by reactions. It is assumed that the electrons provide and receive the energy involved in all reactions.

In Eq. (4), bound-bound, free-bound, and free-free radiation losses are neglected. Bound-bound radiation is of minor importance, as electron impact bound-bound transitions are much faster than the radiative bound-bound processes in this plasma. Free-bound and free-free radiation typically radiate less than 0.01% of the dissipated power.

In Eq. (5), the heavy particle temperature is computed. The first term of this equation describes the temporal behavior of the thermal energy of this gas, in which we use

$$C_h = \tfrac{3}{2}k_B(n_H + n_{H_2} + n_{H^+}). \tag{14}$$

The impact of heat capacity due to ro-vibrational excitation of hydrogen is negligible, as virtually all hydrogen is dissociated before the heavy particles have heated up significantly.

Ignoring the ro-vibrational excitation of molecular hydrogen is justified given that the dissociation is much faster than the excitation in this particular plasma. The heat conductivity λ_h is computed with the mixture rules in Ref. [10].The last term on the left-hand side represents the viscous dissipation. Under the assumption that the plasma is Newtonian, and using the simplification that only velocity components in the radial direction are involved, we can write

$$\overline{\overline{\tau}}:\vec{\nabla}\vec{v}_r = \frac{4}{3}\mu\left[\left(\frac{\partial v_r}{\partial r}\right)^2 - \frac{\partial v_r}{\partial r}\frac{v_r}{r} + \left(\frac{v_r}{r}\right)^2\right]. \tag{15}$$

C. Boundary conditions

For solving these differential equations, it is necessary to have boundary conditions.

The code we use is a two-dimensional (2D) code, which is used solve a one-dimensional (1D) problem. This can be accomplished by setting the boundary conditions in the z direction to homogeneous Neumann conditions. This is not

an efficient method, but as the computational time of our simulation was quite managable (about 1 day on a high-end PC), this is not an important issue.

While most of the other boundary conditions used are quite straightforward, the wall boundary conditions for the temperature are not. We will offer a detailed description of these boundary conditions below.

The wall material is an electrical isolator; hence, the amount of free electrons in this material will be negligible. This means that the plasma electrons do not directly transfer their energy to the wall. The presence of a virtually electron-free plasma sheath further hampers the heat transport by electrons to the wall. We therefore take a homogeneous Neumann boundary condition for the electrons at the wall, that is

$$T_e|_{r_0} = 0. \tag{16}$$

The heavy particles do transfer their heat to the wall. This means that two conditions, namely the continuity of the temperature and of the heat flux, must be simultaneously satisfied,

$$T_h|_{r_0} = T_w|_{r_0} \tag{17}$$

and

$$\left[\lambda_h\left(\frac{\partial T_h}{\partial r} + \frac{T_h}{r}\right)\right]\Bigg|_{r_0} = \left[\lambda_w\left(\frac{\partial T_w}{\partial r} + \frac{T_w}{r}\right)\right]\Bigg|_{r_0}, \tag{18}$$

with r_0 the radius of the channel, T_w the wall temperature and λ_w the heat conductivity of the wall. In order to obtain a useable boundary condition from Eq. (17) and Eq. (18), we must create a model of the heating of the wall to obtain T_w and λ_w.

The heating of the wall is described in a 1D model. We only take into account the temperature changes,

$$\frac{\partial C_w T_w}{\partial t} - \vec{\nabla}\cdot(\lambda_w \vec{\nabla} T_w) = 0, \tag{19}$$

where C_w is the heat capacity of the wall material per cubic meter. It is not possible to solve Eq. (19) analytically, as C_w and λ_w are functions of temperature; therefore, we solve Eq. (19) numerically.

The value of C_w was obtained by fitting Einstein's formula [17] for the specific heat of a solid to measured specific heats of alumina from Ref. [18] in the temperature range from 300 to 600 K,

$$C_w = 3n_w k_B\left[\left(\frac{\theta_E}{T_w}\right)\frac{\exp\left(\frac{\theta_E}{2T_w}\right)}{\exp\left(\frac{\theta_E}{T}\right)-1}\right]^2, \tag{20}$$

with $n_w = 1.17\times10^{29}$ m^{-3} the density of alumina in particles-per cubic meter and $\theta_E = 690$ K the Einstein temperature. The fit was accurate to within 2%.

The value of λ_w was obtained by fitting the theoretical $1/T$ relation for the thermal conductivity at high temperatures [19,20] to measured thermal conductivities of alumina from Ref. [18] in the temperature range between 273 K and 973 K,

$$\lambda_w = \frac{9.5\times10^3\ \mathrm{K}}{T_w}\mathrm{W\ m^{-1}\ K^{-1}}. \tag{21}$$

This expression is expected to be accurate to within 20%.

We do not solve Eq. (19) for the whole wall. Instead, we estimate which part of the wall will be heated significantly by the plasma. This is the innermost 500 nm. As the rest of the material does not heat up significantly, we assume a Dirichlet boundary condition with a value equal to the initial temperature for the outer boundary condition of Eq. (19).

The system of plasma and wall temperature equation is solved by a sequential substitution procedure, which will be sketched. In this procedure, we first solve the plasma equations (1)–(4). Equation (5) is then solved with a Dirichlet boundary condition for the heavy particle temperature. This boundary condition follows from the value of T_w and Eq. (17). From the obtained T_h-field a heat fluxinto the wall is computed. Using Eq. (18), we get a boundary condition for Eq. (19). Solving this equation produces a T_w field. This procedure is repeated until convergence is reached.

D. Adsorbtion of hydrogen on the wall

Alumina can adsorb hydrogen. This hydrogen can be released when the wall is subjected to heating and ion bombardment from the discharge. We do not describe this process in detail; rather, we assume the hydrogen of the wall to be present at startup, evenly distributed throughout the discharge. Provided the hydrogen on the wall is a small fraction of the total hydrogen content, ignoring the release mechanism is not expected to influence the results greatly.

The number of surface sites A_s on the alumina wall can be estimated as

$$A_s = \sqrt[2/3]{n_w} \tag{22}$$

if the surface were a perfectly flat plane. However, this is very likely not to be the case. We multiply the number of surface sites with a factor of 3 to compensate for this, and for the possibility of hydrogen desorbing from deeper layers of the alumina. Assuming every surface site holds one hydrogen atom, the number of hydrogen atoms adsorbed to the capillary wall N_w given by

$$N_w = 2\pi r_0 l A_s. \tag{23}$$

As mentioned, in the model, we distribute this hydrogen through the channel at startup. This leads to an additional hydrogen density due to wall desorption n_{surf} of

$$n_{\mathrm{surf}} = \frac{2N_w}{r_0}. \tag{24}$$

E. The code

For the simulations, we use the PLASIMO code. This code is described in detail in Refs. [12,21–24]. It is a modeling platform that can handle LTE and non-LTE plasmas, currently in two dimensions. Furthermore, its modular structure allows for easy expansion of the code. It has been applied to simulate a wide variety of plasma as described in Refs.

[25–30]. Salient additions for this work include the wall heat transport module and algorithmic changes to improve the treatment of plasmas with very high ionization degree.

III. THE DISCHARGE PARAMETERS

The model we have created is suitable for a wide range of pulsed capillary discharges. In order to validate our model, we will use the specific discharge parameters of an existing pulsed capillary discharge, namely the discharge that is described in Ref. [8]. This discharge was simulated earlier by Bobrova *et al.* [9] using the MHD equations and a generalized Saha equation. The main difference between this approach and our non-LTE approach is that in our approach the finite reaction speed is taken into account.

The capillary under investigation has a radius of 150 μm. The current $I(t)$ is given by

$$I(t) = I_0 \sin\left(\frac{\pi t}{200\ \text{ns}}\right), \quad 0\ \text{ns} < t < 200\ \text{ns} \qquad (25)$$

with I_0 equal to 300 A for the main study. We will also make a parameter study in which I_0 is varied.

There are two contributions to the hydrogen density. The first contribution is the hydrogen prefilling. For this discharge, the initial H_2 density was 1.68×10^{24} m^{-3}. The second contribution is the hydrogen that is liberated from the wall. Using Eq. (24), we obtain that the amount of H_2 from this source is 4.8×10^{23} m^{-3}. The total amount of H_2 is thus 2.16×10^{24} m^{-3}.

In order to initiate the discharge, a small preionization is necessary. The following composition of the initial plasma is assumed: $n_{H_2}=2.0\times10^{24}$ m^{-3}, $n_H=2.8\times10^{23}$ m^{-3}, $n_{H^+}=n_e=4\times10^{21}$ m^{-3}. The initial electron temperature is 1 eV, the initial heavy particle temperature is 25.9 meV (corresponding to 298 K). The plasma is initially at rest and homogeneously distributed in the channel.

IV. RESULTS AND DISCUSSION

A. General results and discussion

The pulsed capillary discharge is simulated using the physical model described in Sec. II for the parameters in Sec. III. Graphs of the electron density, electron temperature, the atomic hydrogen density, and heavy particle temperature as functions of time and radial position are presentend in Fig. 1, Fig. 2, and Fig. 3, respectively. The discharge is strongly dynamic, and based on the plasma parameters, three phases can clearly be distinguished.

(i) The *ionization phase*. Lasting from the startup to about 30 ns, during this phase an almost homogeneous ionization and dissociation of hydrogen takes place.

(ii) The *formation phase*. During this phase, the effect of wall cooling, amplified by the redistribution of current, forms the guiding channel with a hollow electron density profile. This phase lasts from 30 to 60 ns.

(iii) The *guiding phase*. The guiding channel remains relatively stable during this phase, lasting from 60 ns to the end of the simulation.

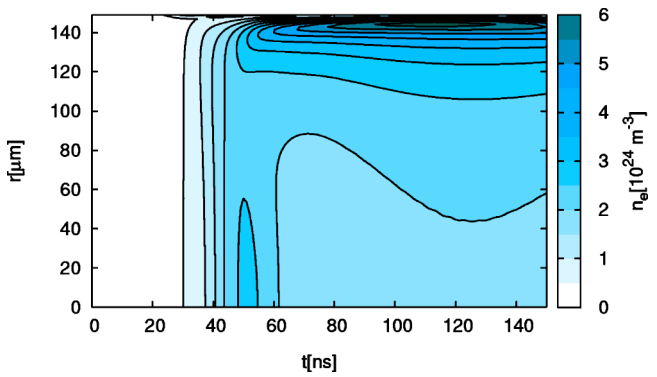

FIG. 1. (Color online) The electron density n_e as a function of time and radial position. The isolines indicate differences of 5×10^{23} m^{-3}.

We will discuss these phases in more detail.

In the ionization phase, during the first few nanoseconds, the electrons heat up. This causes a dramatic rise in the ionization rate and consequently of n_e. The high temperature and increasing electron density rapidly dissociates the molecular hydrogen. The electron density during this phase, from 5 to 30 ns, increases far more rapidly than the power, which implies that the electron temperature drops slightly, from around 3 eV at 5 ns to 1.7 eV at 30 ns. This behavior is a result of the finite reactionspeed which is used in a non-LTE approach; in a 2-temperature Saha approach, the electron temperature rises during this phase [9]. In our model, the rise of the heavy particle temperature is initially quite slow, as electron-neutral collisions are not very effective in transferring heat from the electrons to the heavy particles.

In the formation phase, wall cooling shapes the channel. The heavy particles are directly cooled at the wall. However, heat transfer from the electrons to the heavy particles also cools the electrons here. This causes the ionization to be reduced locally. Furthermore, the reduced ionization means that the local electrical conductivity is lower, causing less current to flow which leads to a reduced Ohmic dissipation in the wall region. This further amplifies the temperature drop at the wall.

The higher T_h, T_e, and n_e in the center all cause the pressure there to be much higher than at the wall. This causes a

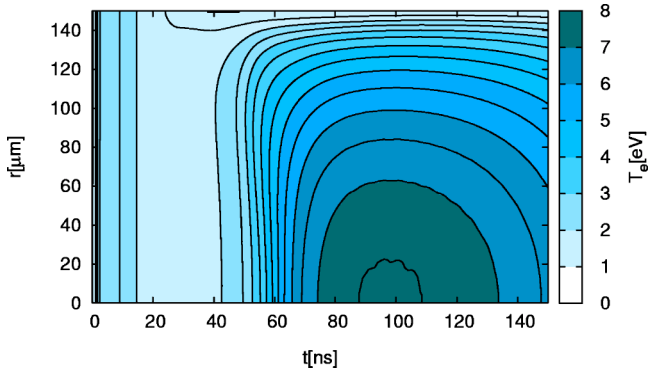

FIG. 2. (Color online) The electron temperature T_e as a function of time and radial position. The isolines indicate differences of 0.5 eV.

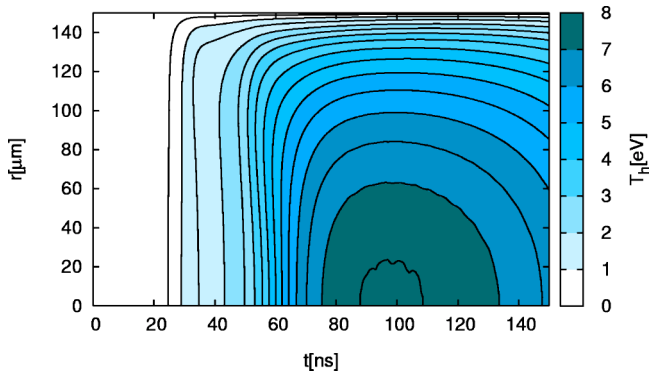

FIG. 3. (Color online) The heavy particle temperature T_h as a function of time and radial position. The isolines indicate differences of 0.5 eV.

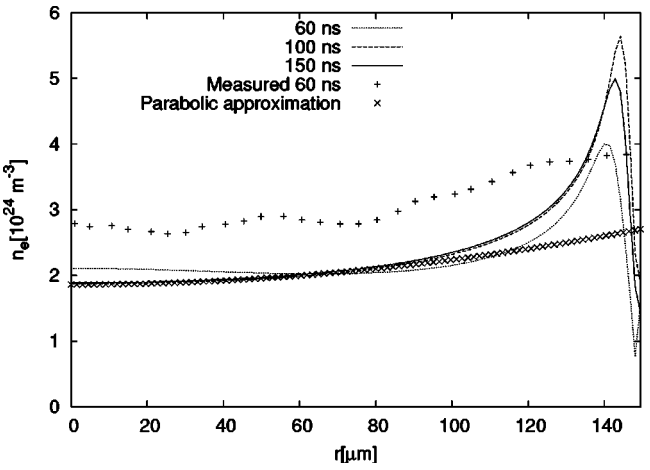

FIG. 4. The computed n_e as a function of radius at various times, compared with experimental results from Ref. [8]. Furthermore, a parabolic approximation of n_e in the central part of the discharge is given. The function describing the parabolic approximation is given in Eq. (26).

bulk flow from the center to the wall. Maximum velocities are reached in the order of 2×10^3 m s^{-1}. Comparing this with the thermal velocity leads to a Mach number which can reach values of up to $M=0.15$, meaning that the flow remains subsonic. During this phase, the ionization degree keeps rising. The central ionization degree is well above 99% at 60 ns. T_e starts rising again, especially when the plasma is nearly fully ionized, as no more energy is consumed by further ionization. T_h also rises due to the higher collision frequency between electrons and ions. It becomes almost equal to the electron temperature at 40 ns, except near the wall. From this time onward, n_e is nearly equal to the value predicted by the Saha equation with the temperature given by T_e [31].

The lower temperature at the wall has two opposing effects on n_e. The total particle density, and therefore the electron density, becomes higher because the pressure remains roughly equal in the channel. However, the lower temperature at the wall meansthe plasma is not fully ionized near the wall.

The creation of pressure differences is amplified by redistribution of current. The higher temperature in the center causes higher conductivity there, which causes a higher local current density. The net effect of this is an increased Ohmic dissipation density, causing further increases in central temperature and pressure.

During the stable phase, the plasma parameters remain roughly stable over tens of nanoseconds. The ionization degree is well over 99%, except in the outer 10 μm of the channel, where the ionization degree drops rapidly, to a few percent near the wall. As long as the laser does not come close to the walls, this is not expected to be detrimental, as the center is fully ionized. The total average ionization degree is around 56% at 60 ns.

B. Error analysis and comparison with experiments

We will consider the most important sources of error in the model and discuss their impact on the plasma parameters. Furthermore, we will compare our model results with the experiment.

The key plasma parameters n_e, T_e, and T_h are remarkably robust with respect to variations in the typically rather inaccurate reaction rates and transport coefficients.

With respect to the reaction rates, we note that the equilibrium composition is not influenced by the reaction rates, as backward and forward rate are linked via detailed balancing. The reaction rate would impact the electron temperature and density during startup.

The most important transport coefficients for the formation of the channel are the electrical conductivity, and the thermal conductivity. Because there is a strong positive correlation between temperature and the loss term (thermal conductivity) and a strong negative correlation to the the production term (ohmic dissipation), errors in the transport coefficients cause only small errors in the temperature fields.

There are two aspects of the model which could be improved.

(i) Diffusion is not included. While the typical diffusion time scales are slower than the other typical time scales of the discharge, it is expected to have an effect on the plasma parameters, especially near the wall.

(ii) A better model of the hydrogen desorbing from the wall could reduce the uncertainty in the amount of hydrogen which is in the discharge.

Given these uncertainties, we do expect the model to predict electron densities with an accuracy of about 30%, and the temperatures with an accuracy of about 10%.

In order to verify the validity of our model, we compare the modeling results with the experimental results published in Ref. [8] in Fig. 4. Given that the error in the measurements are claimed to be 12%, thequantitative agreement between the electron density in experiment and model is satisfactory. The sharp peaks in the electron density near the wall, a result of the lower temperature near the wall, are absent in the measurements.

C. Suitability for guiding

For the guiding of a laser, the electron density profile is the key parameter. A graph of the electron density at various

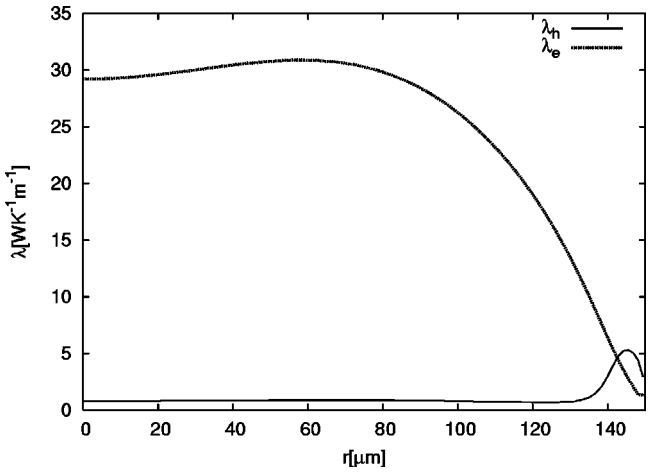

FIG. 5. The electron thermal conductivity λ_e and the heavy particle heat conductivity λ_h as a function of the radius at 100 ns. In most of the plasma, the lighter electrons cause most of the heat transport. However, near the wall, the lower electron density and higher heavy particle density cause the λ_h to be larger than λ_e.

times as a function of the radius is given in Fig. 4. As can be seen, during the guiding phase, the electron density profile only superficially resembles a parabola; it is much flatter in the center. This is caused by the heat conductivity, which is much higher in the center than near the wall. This causes the temperature gradients to be smaller in the center and hence the temperature profile to be flatter. This, in turn, makes the electron density profile flatter. A graph of λ_h and λ_e at 100 ns is shown in Fig. 5, while a graph of T_e and T_h at 100 ns is shown in Fig. 6.

While the electron density over the whole channel does not resemble a parabola, the electron density in the central region of the channel does. For $r<90$ μm and $t>80$ ns, the central density n_e^c can be described well by

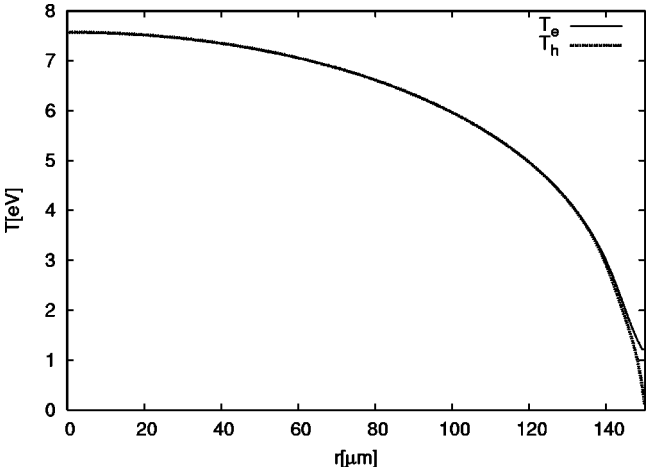

FIG. 6. The heavy particle temperature T_h and the electron temperature T_e as a function of the radius at 100 ns. Both T_e and T_h have rather flat profiles in the center. Near the wall, both temperatures differ significantly.

$$n_e^c = \left[0.85\left(\frac{r}{r_0}\right)^2 + 1.86\right] \times 10^{-24}\ \mathrm{m}^3. \tag{26}$$

For a Gaussian beam, the matched spot size W is given by [9]

$$W = \left(0.5\pi r_e \frac{\partial^2 n_e}{\partial r^2}\right)^{-1/4} \tag{27}$$

with r_e the classical electron radius which has a numerical value of 2.817×10^{-15} m. Combining Eq. (26) and Eq. (27) gives a matched spot size of 42 μm. Because the matched spot size is much smaller than the part of the discharge in which the electron density is approximately parabolic, the fact that the electron densityis not parabolic over the whole channel is of little importance for guiding.

Excessive heating of the wall during the discharge might cause the practical problem of loss of wall material, thus reducing capillary lifetime and polluting the plasma with elements that cannot be fully stripped of electrons by the plasma. Furthermore, it will lead to cooling of the plasma. The temperature of the wall-plasma interface, which is the hottest point of the wall, reaches its highest value of 1780 K at $t=153$ ns. This is still well below the melting point of alumina. Furthermore, the low electron temperature near the wall means that ions impact the wall with little energy [32], meaning there is little sputtering. Hence, we expect very long capillary lifetimes, which is also found in the experiments [8]. This is important for practical applications.

D. The effect of non-LTE

As discussed, one of the main differences between our work and the earlier work of Bobrova *et al.* [9] is our adoption of a non-LTE model as opposed to a two-temperature magneto-hydrodynamic (MHD) system where the free energy is minimized. We will explore two non-LTE effects: the effect of the finite reaction speed on composition and the temperature difference between electrons and ions.

One of the effects of the finite reaction speed is an electron density which differs from the Saha density. We present the overpopulation of the electron density and the Saha density as a function of time for various radial positions in Fig. 7. This figure shows that during the startup phase, n_e is much lower than the Saha density. It takes about 60 ns for the electron density to reach the Saha density. This is in line with the estimated reaction speeds, which are in the order of 10^8 Hz.

The finite heat transfer rate between electrons and ions allows the electrons to have a different temperature than the ions. We present the difference between the electron and ion temperature as a function of time for various radial positions in Fig. 8. As can be seen, the difference between T_e and T_h rises sharply during the first few nanoseconds, as T_e rises while T_h remains almost constant. After this phase, T_e remains roughly constant until about 30 ns, while T_h rises due to the heat flow from the electrons. While the rising ionization degree increases the collision frequency and hence k_{heat}, the decreasing difference between T_e and T_h roughly compensates for this, causing a roughly linear decrease of T_e-T_h

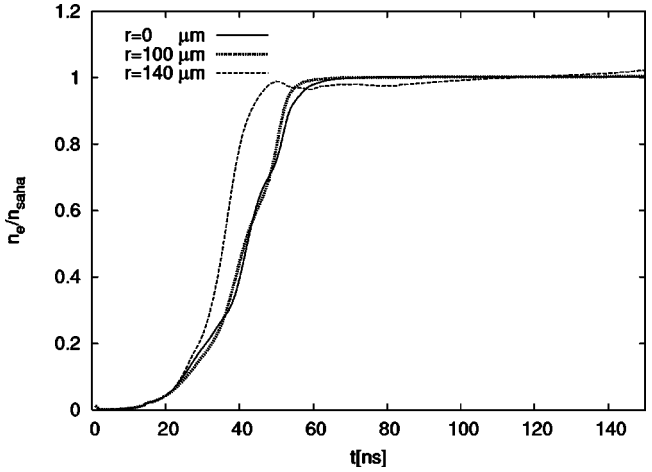

FIG. 7. The ratio of the electron density and the Saha density as a function of time, at three different radial positions.

until the difference becomes negligible. The bump of T_e-T_h at the center of the channel at about 60 ns is the result of the redistribution of current to the center.

E. A parameter study with varying current

In the previous part of the discussion, a particular example of the pulsed capillary discharge has been simulated, and the results discussed and explained in great detail. Having established that our model produces physically relevant results for this case, we will now use this model to perform a parameter study by varying I_0 between 200 and 500 A.

We will restrict ourselves to the discussion of the result that is the most relevant for the guiding properties, n_e as a function of r, at $t=80$ ns. At this time, all channels that were under investigation reached the stable phase. Graphs of n_e as a function of r for selected currents (200 A, 350 A, and 500 A) are given in Fig. 9.

For all the values of the current that were investigated, a parabolic approximation of n_e^c, described by

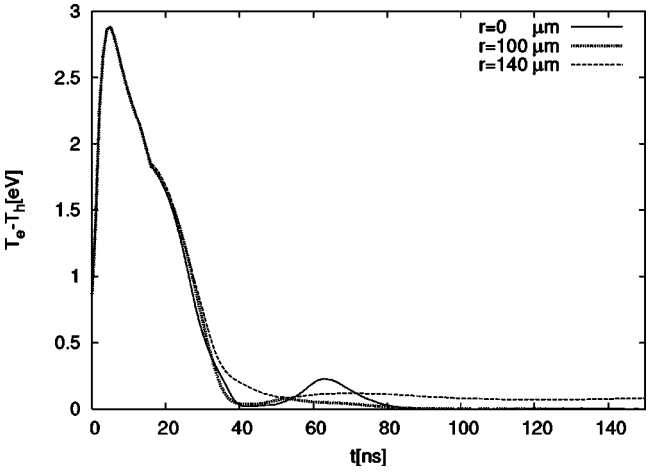

FIG. 8. The difference between T_e and T_h as a function of time, at three different radial positions.

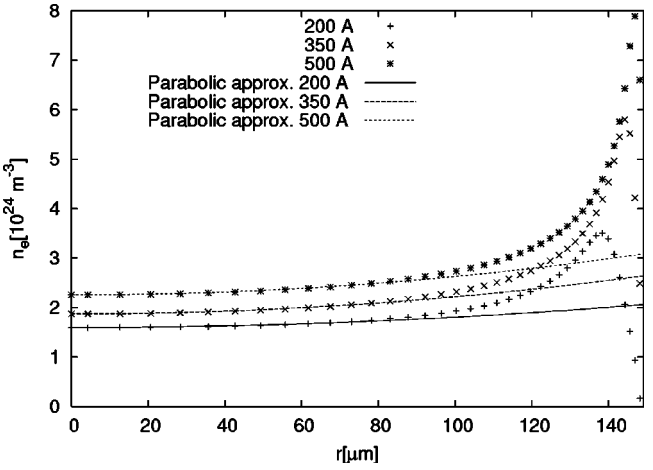

FIG. 9. The computed electron density n_e as a function of radius for three different currents. Furthermore, a parabolic approximation in the central part of the discharge is given.

$$n_e^c = \left(a + b\left(\frac{r}{r_0}\right)^2\right) \times 10^{-24}\ \mathrm{m}^{-3}, \tag{28}$$

with a a fit parameter and b the central density was fitted to the results. These curves are also drawn in Fig. 9. For all investigated currents, the values of a and b are given in Table I.

From Fig. 9, we see that the match between the parabolic fit and the computed values of n_e is good for $r<90$ μm. As discussed, this means that the channel is wide enough for laser guiding. It can be clearly seenthat the maximum of the electron density shifts outwards and reaches a higher value for higher current. This is caused by the higher temperature near the wall, which causes a higher degree of ionization near the wall. Because a hydrogen ion plus a hydrogen electron produce more pressure for a given temperature than a hydrogen atom, the density near the wall is lower for a higher current, causing the central density to be higher. This trend is clear in the values of a in Table I.

Generally, the curvature of the channel b did not depend strongly on the current, as can be seen in Table I, with the exception of the lowest value of the current, 200 A. For this current, a significant part of the channel is not fully ionized. The relative insensitivity of b to the value of the current I

TABLE I. The parameters a and b of a the parabolic approximation of the electron density in the central part of the channel, for various currents. a and b are defined in Eq. (28).

Current (A)	a	b
200	1.60	0.47
250	1.62	0.72
300	1.74	0.75
350	1.87	0.78
400	2.00	0.80
450	2.13	0.82
500	2.26	0.84

makes I a poor choice for tuning the guiding behavior of the channel, especially given that W is proportional to $b^{-1/4}$ as described in Eq. (27).

A practical problem when increasing the current is the heating of the wall. While the wall termperature stays below the melting point of alumina of 2326 K [18] for the default current of 300 A, the wall material may melt for higher values of the current. Note that this does not influence the results presented here, as the results are taken at $t=80$ ns, well before the wall temperature reaches the melting point of alumina. At temperatures above the melting point, the wall model cannot accurately predict the temperatures anymore, as Eq. (20) and Eq. (21) are valid for solids only. A precise prediction of the current at which evaporation of wall material becomes significant is beyond the scope of this study.

V. CONCLUSIONS

We have presented a theoretical model suitable for simulating a slow capillary discharge in hydrogen. This model has been used to simulate the discharge described in Ref. [8].

The model uses a non-LTE description, which has not yet been used for the description of these types of discharges to our knowledge. Previous models [9] used a two-temperature approach in which the free energy was minimized. Theadvantage of the current approach is that the effect of the finite reaction speed can be included. The heating of the wall is also numerically described, and the plasma and wall models are coupled.

The model predicts three distinctive phases in the discharge.

(i) The ionization phase. During this phase, the plasma ionizes roughly homogeneously. It lasts about 30 ns for the discharge under study. The finite reaction speed causes the electron temperature to drop, rather than rise, from 5 to 30 ns.

(ii) The formation phase. Heat conductivity to the wall, becoming more significant with rising ionization and temperatures, starts to create significant temperature and pressure gradients. Bulk flow, which remains subsonic, counteracts this, causing a bulk density gradient, and, given the almost homogeneous full ionization, a hollow electron density profile. This phase lasts up to 60 ns.

(iii) The stable phase. With the Ohmic dissipation and heat conductivity roughly balancing, and the plasma close to Saha equilibrium, the plasma enters a phase during which the plasma parameters are roughly stable over many tens of nanoseconds The heating of the wall and the changing current cause slow variations in the plasma parameters. Given that a stable, fully ionized channel with a hollow electron density profile is formed for much longer than the sub-ns time it takes for the laser to pass, we expect this phase to be most suitable for guiding.

The model is expected to predict the electron density with an accuracy of 30%. Comparison of the model results with measurements [8] gives satisfactory agreement. This indicates that the used model is indeed suitable for the computation of pulsed capillary discharges.

The wall of the plasma heats up significantly, up to a temperature of 1780 K. This means however that the wall will not melt, which is desirable from a practical point of view. Furthermore, the magnitude of the wall heating demands that a robust and accurate model is used to describe it, such as the one used in this work.

The fact that the thermal conductivity is much higher in the center than near the wall causes the temperature, and thus the electron density profile, to be much flatter in the center than near the wall. This means that the that is not truly parabolic, butmore blocklike. However, as the central part of the profile is nearly parabolic, this is not expected to be detrimental to guiding.

A parameter study in which the current was varied has been carried out. It was found that the influence of the current on the key guiding parameters is small, especially for currents above 250 A. Excessive wall heating might be detrimental to the practical use of currents above 300 A.

ACKNOWLEDGMENTS

The authors would like to thank Zahoor Ahmad, Wang Chunmei, and Elena Toma for the fruitful discussions. The PLASIMO team members, current and former, are acknowledged for their contributions to the code. This work was performed as part of the research program of Stichting voor Fundamenteel Onderzoek der Materie (FOM) with financial support from NWO, within FOM program 55 on Laser Wakefield Accelerators.

[1] T. Tajima and J. M. Dawson, Phys. Rev. Lett. **43**, 267 (1979).
[2] E. Esaray, P. Sprangle, J. Krall, and A. Ting, IEEE Trans. Plasma Sci. **24**, 252 (1996).
[3] C. Wang, R. Keppens, and J. P. Goedbloed, J. Phys. D **36**, 2255 (2003).
[4] Y. Ehrlich, C. Cohen, A. Zigler, J. Krall, P. Sprangle, and E. Esaray, Phys. Rev. Lett. **77**, 4186 (1996).
[5] J. J. Rocca, V. Shlyaptsev, F. G. Tomasel, O. D. Cortazar, D. Hartshorn, and J. L. A. Chilla, Phys. Rev. Lett. **73**, 2192 (1994).
[6] K. Nakajima, Nucl. Instrum. Methods Phys. Res. A **455**, 140 (2000).
[7] M. C. Marconi, C. H. Moreno, J. J. Rocca, V. N. Shlyaptsev, and A. L. Osterheld, Phys. Rev. E **62**, 7209 (2000).
[8] J. D. Spence and S. M. Hooker, Phys. Rev. E **63**, 015401(R) (2001).
[9] N. A. Bobrova, A. A. Esaulov, J. I. Sakai, P. V. Sasorov, D. J. Spence, A. Butler, S. M. Hooker, and S. V. Bulanov, Phys. Rev. E **65**, 016407 (2002).
[10] M. Mitchner and C. H. Kruger, *Partially Ionized Gasses* (Wiley, New York, 1983).
[11] C. A. Ordonez and M. I. Molina, Phys. Plasmas **1**, 2515

(1994).
[12] J. van Dijk, Ph.D. thesis, Eindhoven University of Technology, 2001.
[13] C. Trevisan and J. Tennyson, Plasma Phys. Controlled Fusion **44**, 1263 (2002).
[14] R. K. Janev, W. D. Langer, K. Evands, Jr., and D. E. Post, Jr., *Elementary Processes in Hydrogen-Helium Discharges* (Springer-Verlag, New York, 1987).
[15] J. van der Mullen and J. Jonkers, Spectrochim. Acta, Part B **54**, 1017 (1999).
[16] L. S. Frost, J. Appl. Phys. **32**, 2029 (1961).
[17] P. W. Atkins, *Physical Chemistry* (Oxford University Press, Oxford, 1998).
[18] CRC Handbook of Chemistry and Phyiscs, edited by D. R. Lide, (CRC Press, Boca Raton, FL, 2004).
[19] C. Kittel, *Introduction to Solid State Physics* (Wiley, New York, 1996).
[20] J. M. Ziman, *Electrons and Phonons* (Oxford, New York 1960).
[21] G. M. Janssen, Ph.D. thesis, Eindhoven University of Technology, 2000.
[22] H. van der Heijden, Ph.D. thesis, Eindhoven University of Technology, 2002.
[23] A. Hartgers, Ph.D. thesis, Eindhoven University of Technology, 2003.
[24] http://plasimo.phys.tue.nl/
[25] K. T. A. L. Burm, W. J. Goedheer, J. A. M. van der Mullen, G. M. Janssen, and D. C. Schram, Plasma Sources Sci. Technol. **7**, 395 (1998).
[26] G. M. Janssen, J. van Dijk, D. A. Benoy, M. A. Tas, K. T. A. L. Burm, W. J. Goedheer, J. A. M. van der Mullen, and D. C. Schram, Plasma Sources Sci. Technol. **8**, 1 (1999).
[27] H. van der Heijden and J. van der Mullen, J. Phys. B **34**, 4183 (2001).
[28] H. van der Heijden, J. Baier, and J. van der Mullen, J. Phys. B **35**, 3633 (2002).
[29] H. van der Heijden and J. van der Mullen, J. Phys. D **35**, 2112 (2002).
[30] J. van Dijk, M. van der Velden, and J. van der Mullen, J. Phys. D **35**, 2748 (2002).
[31] J. A. M. van der Mullen, D. A. Benoy, F. H. A. G. Fey, B. van der Sijde, and J. Vlček, Phys. Rev. E **50**, 3925 (1994).
[32] M. A. Lieberman and A. J. Lichtenberg, *Principles of Plasma Discharges and Materials Processing* (Wiley, New York, 1994).